INTERNATIONAL JOURNAL OF
Minerals, Metallurgy and Materials

*Volume 31, Number 10, October 2024*
*Page 2199*

Research Article https://doi.org/10.1007/s12613-024-2887-7

# Effect of two-step solid solution on microstructure and δ phase precipitation of Inconel 718 alloy

*Enyu Liu*[1,2),*], *Qingshuang Ma*[1,2),*], *Xintong Li*[1,2)], *Aoxue Gao*[1,2)], *Jing Bai*[1,2)], *Liming Yu*[3)], *Qiuzhi Gao*[1,2),✉], *and Huijun Li*[3,4),✉]

1) School of Materials Science and Engineering, Northeastern University, Shenyang 110819, China
2) School of Resources and Materials, Northeastern University at Qinhuangdao, Qinhuangdao 066004, China
3) School of Materials Science & Engineering, Tianjin University, Tianjin 300354, China
4) School of Mechanical, Materials and Mechatronic Engineering, University of Wollongong, Wollongong, NSW 2522, Australia
(Received: 23 January 2024; revised: 6 March 2024; accepted: 20 March 2024)

**Abstract:** Inconel 718 is the most popular nickel-based superalloy and is extensively used in aerospace, automotive, and energy industries owing to its extraordinary thermomechanical properties. The effects of different two-step solid solution treatments on microstructure and δ phase precipitation of Inconel 718 alloy were studied, and the transformation mechanism from γ″ metastable phase to δ phase was clarified. The precipitates were statistically analyzed by X-ray diffractometry. The results show that the δ phase content firstly increased, and then decreased with the temperature of the second-step solid solution. The changes in microstructure and δ phase were studied by scanning electron microscopy and transmission electron microscopy. An intragranular δ phase formed in Inconel 718 alloy at the second-step solid solution temperature of 925°C, and its orientation relationship with γ matrix was determined as $//[01\bar{1}]_{\gamma}$ and $(010)_{\delta}//(111)_{\gamma}$. Furthermore, the Vickers hardness of different heat treatment samples was measured, and the sample treated by second-step solid solution at 1010°C reached the maximum hardness of HV 446.84.

**Keywords:** Inconel 718 alloy; two-step solid solution treatment; δ phase; γ″–δ transformation

## 1. Introduction

Applied since the 1960s, Inconel 718 alloy has emerged as the most successful nickel-based wrought superalloy for aeroengines [1]. This precipitation-strengthened nickel–iron-based alloy possesses better forging and welding properties than other wrought superalloys [2–4]. Additionally, it exhibits excellent fatigue and creep rupture properties. The combination of these desirable mechanical properties and its flexible machinability has made Inconel 718 the globally preferred material for elevated temperature applications and static/rotating loads, such as in turbine disks, compressor disks, guide vanes, fastening bolts, and pipes [5–7].

Inconel 718 alloy is a typical precipitation-strengthened superalloy with γ″-$Ni_3Nb$ ($D0_{22}$) and $L1_2$ ordered γ′-$Ni_3$(Al,Ti) phases precipitated on γ matrix (face-centered cubic, FCC) [8–9]. During certain heat treatments and long-term service, δ-$Ni_3Nb$ ($D0_a$) precipitates along grain boundaries and within grains. The main precipitates of Inconel 718 alloy are γ″, γ′, and δ phases, which have a decisive influence on its processing and service properties [10–11]. In particular, γ″ phase is metastable and can transform into a noncoherent, stable δ phase with an orthorhombic structure when exposed to temperatures exceeding 650°C for extended periods [12–15]. Precipitating an appropriate amount of δ phase at the grain boundary can inhibit grain growth and improve the ductility of the material. However, intracrystalline δ phase is a harmful phase, resulting in significant hardening and increased brittleness of the material. Therefore, studying the precipitation behavior of δ phase and the transformation mechanism of γ″ to δ phase during heat treatment is necessary to improve the properties of materials [16–17].

Research on Inconel 718 alloy focuses on the comparative analysis of existing heat treatment systems, evolutions of precipitation phase, and performance after aging [18–23]. Bai *et al.* [24] and Rao *et al.* [25] revealed that solution temperature has a significant impact on the microstructure and properties of Inconel 718 alloy. With increasing solution temperature, the δ phase content increases first and then decreases. In addition, increasing the solution temperature can significantly improve the stress fracture life and fracture ductility of the alloy. An *et al.* [26] found that after two-stage solid solution treatment, the grain growth is effectively controlled, and the δ phase precipitation is promoted. Cao *et al.* [9] and Theska *et al.* [27] further observed that during two-stage aging, coarse γ″ phases also form with the precipitation of

*These authors contributed equally to this work.
✉ Corresponding authors: Qiuzhi Gao E-mail: neuqgao@163.com; Huijun Li E-mail: huijun@uow.edu.au

Springer

fine γ″ phases. In addition, conventional aging heat treatment at 900°C can result in the precipitation of coarse γ″ phase. With duration of aging, the coarse γ″ phase is completely replaced by the δ phase [28]. In summary, solid solution and aging treatments have an important and complex influence on the δ phase precipitation in Inconel 718 alloy.

Inconel 718 alloy is usually delivered in a solid solution state for practical applications, and solid solution and aging treatments are carried out again after subsequent welding or machining, resulting in a two-step solid solution and aging heat treatment [29]. In addition, the two-step solid solution can promote the formation of δ phase, control its morphology and distribution, and obtain alloys with different δ phase contents. Therefore, the effects of second-step solid solution temperature on the precipitation of δ phase and the transformation of γ″ to δ phase were studied. In this work, the experimental solid solution time was selected as the holding time of the two-step solid solution treatment, and the holding time of each group was the same. The second-step solid solution temperature was determined according to the precipitation temperature of the δ phase. Given that 960°C is the peak temperature of δ phase precipitation, the second-step solid solution temperature must be higher or lower than this temperature. A small temperature interval was used to observe and control the effect of solution temperature on the precipitation and transformation of δ phase.

In this study, the effect of two-step solution treatment on the microstructure and δ phase precipitation of Inconel 718 alloy was systematically investigated. The evolution of δ phase and its effect on Vickers hardness during the two-step solution treatment were studied. In addition, the transformation mechanism of γ″ metastable phase to δ phase was clarified. The results provide a significant reference for optimizing the microstructure and heat treatment of Inconel 718.

## 2. Experimental

The experimental material was commercially forged Inconel 718 alloy produced by Baoshan Iron & Steel Corporation, China, using vacuum induction melting and vacuum arc remelting techniques, followed by homogenization at 1200°C for 24 h. The chemical composition of the material is shown in Table 1. After multipass high-temperature forging deformation, a bar with a diameter of 65 mm was finally obtained. The samples were subjected to two-step solid solution and aging treatment to study the effects of the δ phase on the alloy. For the two-step solid solution, the first step was performed at a solution temperature of 980°C for 1 h, followed by water cooling (WC). The second step was performed at temperatures of 925, 940, 954, 968, 980, and 1010°C for 1 h each, followed by air cooling (AC). After the solid solution treatment, an aging treatment was carried out. The temperature was held at 720°C for 8 h, followed by furnace cooling (FC) to 620°C for 8 h and AC. All these treatments were carried out in a box furnace, and the detailed settings are listed in Table 2. The samples subjected to the two-step solid solution treatment were distinguished by the second-step solid solution temperature, and the comparison samples without two-step solid solution treatment were named "AGE."

After mechanical grinding and polishing, the samples with different treatments were corroded at room temperature for 8 min in the corrosive solution of 5 g of $CuCl_2$ + 100 mL of HCl + 100 mL of $CH_3CH_2OH$. The microstructure and precipitate morphology after heat treatment were characterized by a Leica-DMI 5000 M optical microscope (OM) and SUPRA55 SAPPHIRE field emission scanning electron microscope (SEM). The heat-treated samples were thinly sliced into 0.3 mm-thick pieces and then mechanically grounded to 50–70 μm. Double spray thinning was performed with a solution of 5vol% $HClO_4$ and 95vol% $CH_3CH_2OH$ for transmission electron microscopy (TEM) characterization. The morphology, composition, and crystal structure of the precipitated phase were characterized by JEM-2100 F TEM with an operating voltage of 40 V and temperature of −20°C. X-ray diffraction (XRD) with a scanning step of 0.02° was measured by a SMARTLAB X-ray diffractometer to determine the type of precipitates. The particle size and volume fraction of precipitates were quantitatively analyzed with Nano Measurer and Image J software. The hardness of the samples was tested five times using an MHV-50Z/V2.0 digital Vickers hardness tester with a load of 49 N and holding for 10 s, and the measurements were averaged.

**Table 1. Chemical composition of Inconel 718 alloy** wt%

| Ni | Cr | Nb + Ta | Mo | Ti | Al | Co | C | S | P | O | N | Fe |
|---|---|---|---|---|---|---|---|---|---|---|---|---|
| 52.63 | 19.00 | 5.05 | 3.09 | 1.02 | 0.51 | 0.02 | 0.02 | <0.01 | <0.01 | <0.01 | <0.01 | Bal. |

**Table 2. Heat treatment settings of Inconel 718 alloy**

| Sample | First-step solid solution | Second-step solid solution | Aging |
|---|---|---|---|
| AGE | 980°C, 1 h, WC | None | 720°C, 8 h, FC to 620°C, 8 h, AC |
| G925 | | 925°C, 1 h, AC | |
| G940 | | 940°C, 1 h, AC | |
| G954 | | 954°C, 1 h, AC | |
| G968 | | 968°C, 1 h, AC | |
| G980 | | 980°C, 1 h, AC | |
| G1010 | | 1010°C, 1 h, AC | |

## 3. Results and discussion

### 3.1. Effect of second-step solid solution temperature on microstructure of the alloy

For comparative analysis, the microstructure of Inconel 718 alloy was observed after different heat treatments. Fig. 1 shows the microstructure images of AGE. After a single solution and aging treatment, the alloy consists of typical equiaxed grains, some twins in γ-matrix, and short rod-like δ precipitates at grain boundaries [30–32]. According to the calculation, the average grain diameter is 9–11 μm, the grain size grade is 10–11, and the δ phase content is 1.67vol%.

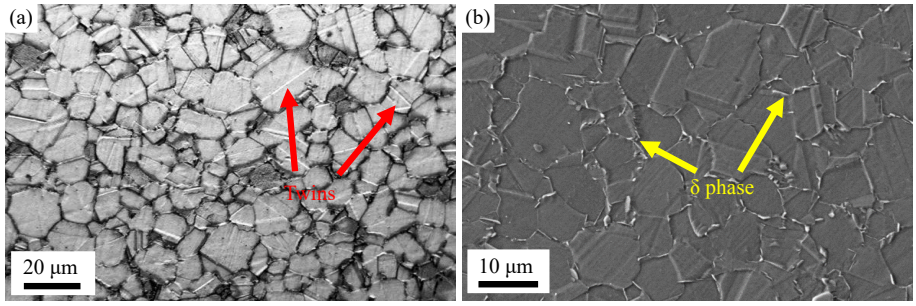


**Fig. 1. Microstructure of Inconel 718 alloy after single solution and aging treatment: (a) OM image, (b) SEM image.**

The microstructure evolution after different two-step solid solution treatments is shown in Fig. 2. Except for the change in grain size, no significant difference in microstructure is observed. The average grain diameter and grain size grade of Inconel 718 alloy under different heat treatment conditions were calculated based on the intercept method, as shown in Table 3. As the second-step solid solution temperature increases from 925 to 1010°C, the average grain diameter of Inconel 718 alloy increases first, then decreases and finally stabilizes. Meanwhile, the grain size grade does not change much. These results demonstrate that the applied two-step solid solution treatment is adequate, and the grains of γ-matrix do not overgrow with the increase in the second-step solid solution temperature.

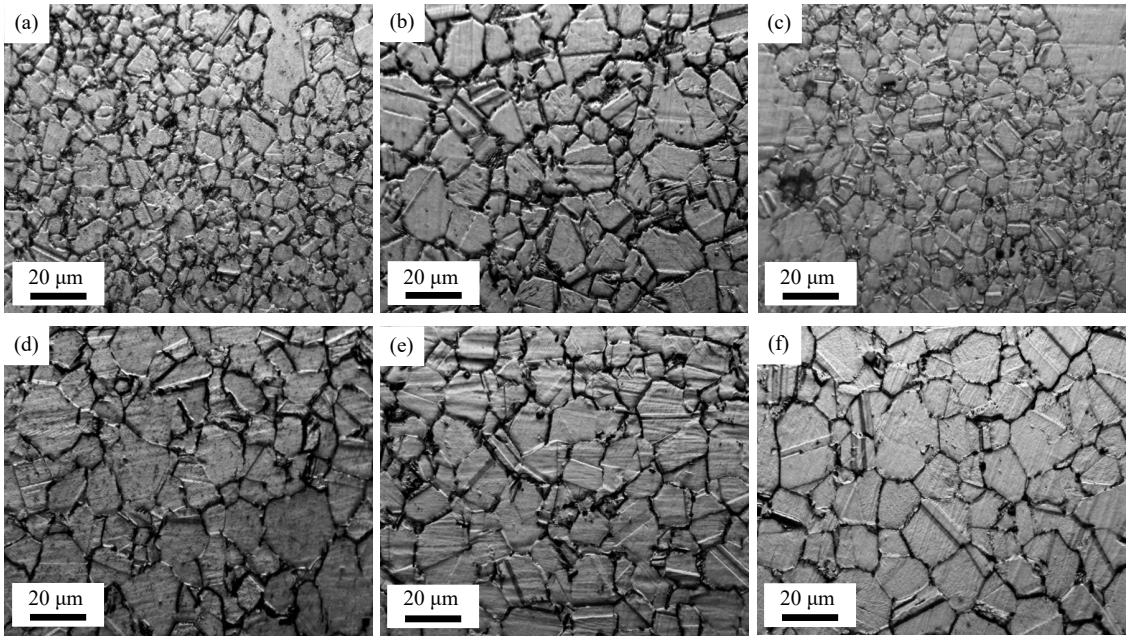


**Fig. 2. OM images of Inconel 718 alloy with different two-step solid solution treatments: (a) G925, (b) G940, (c) G954, (d) G968, (e) G980, and (f) G1010.**

Fig. 3 shows the SEM images of Inconel 718 alloy after different two-step solid solution treatments and aging treatments. In each state, the δ phase is still distributed along the grain boundaries in the form of short rods or needles, but its content differs. Table 4 shows the statistical results from the semiquantitative analysis of δ phase content in Inconel 718 alloy after different two-step solid solution treatments obtained from the image analysis software Image-Pro. After treatment with second-step solid solution temperature at 925, 940, 954, and 968°C, the δ phase content becomes higher than that of AGE state. In addition, the δ phase content increases gradually with the second-step solid solution temperature before 954°C and then decreases gradually with the increase in the second-step solid solution temperature. After the two-step solid solution treatment at 980°C, the δ phase on the local grain boundaries dissolves again. After the two-step solid solution treatment at 1010°C, the δ phase dissolves in a large amount. This phenomenon is consistent with the trans-

**Table 3. Average grain diameter and grain size grade of Inconel 718 alloy after different two-step solid solution treatments**

| Sample | Average grain diameter / μm | Grain size grade |
|---|---|---|
| G925 | 5.6–7.9 | 11–12 |
| G940 | 11.8–15.9 | 9–10 |
| G954 | 7.9–11.2 | 10–11 |
| G968 | 11.2–13.5 | 9–10 |
| G980 | 11.2–15.9 | 9–10 |
| G1010 | 12.5–15.9 | 9–10 |

formation of Inconel 718 alloy that dissolves and precipitates with temperature and time [33]. The precipitation peak of the δ phase appears approximately at 950°C, then begins to dissolve at 980°C and completely dissolves at 1020°C.

The microstructure under metallographic and scanning electron microscopy reveals that from 925 to 1010°C, the second-step solid solution temperature has no significant effect on the grain size grade and morphology of Inconel 718 alloy. The grain size grade does not change much, and the δ phase precipitation increases first and then decreases. Analysis of the variation of average grain diameter and δ phase content shows that the average grain diameter gradually increases with the second-step solid solution temperature. Owing to δ phase precipitation, the grain growth is inhibited, and the grain diameter tends to be stable. Given that the δ phase precipitation is the highest in G954, which greatly inhibits grain growth, the average grain diameter of G954 is small, and the grain size grade is high.

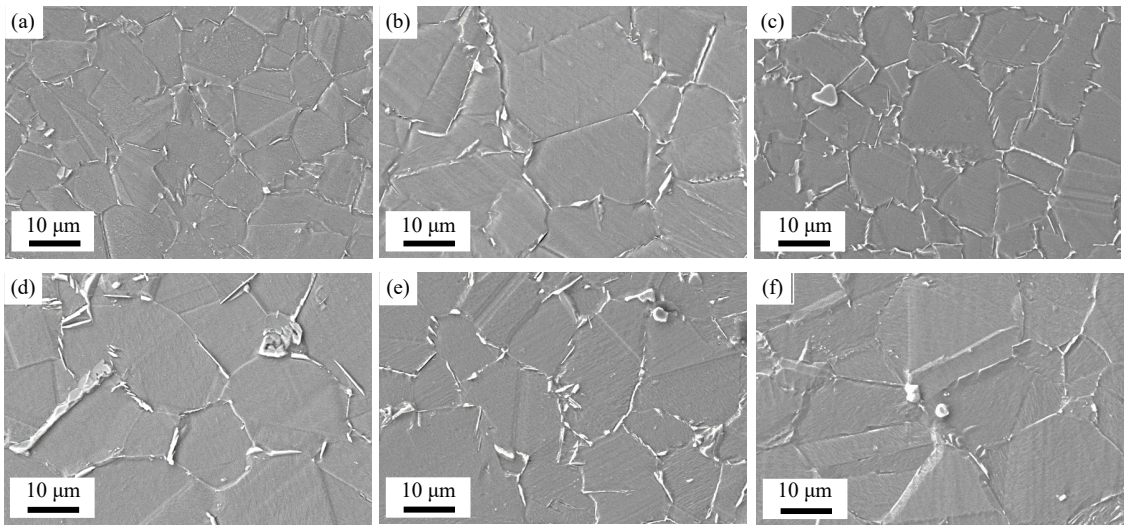


**Fig. 3. SEM images of Inconel 718 alloy after different two-step solid solution treatments: (a) G925, (b) G940, (c) G954, (d) G968, (e) G980, and (f) G1010.**

The content of each precipitated phase under different heat treatment conditions was quantitatively calculated by XRD phase analysis to study the effects of second-step solid solution temperature on precipitates. Fig. 4 shows the XRD pattern of Inconel 718 alloy after different two-step solid solution treatments and aging. In addition to the main peaks of austenite (γ phase, γ′ phase, and γ″ phase), the diffraction peak of δ-$Ni_3Nb$ phase is found to be around 45.6°. Other precipitates cannot be detected. Given that the δ phase has redissolved under 1010°C, its diffraction peak cannot be detected.

**Table 4. Volume fraction of δ phase after different two-step solid solution treatments**

| Sample | Volume fraction of δ phase / % |
|---|---|
| AGE | 1.67 |
| G925 | 2.47 |
| G940 | 2.89 |
| G954 | 3.79 |
| G968 | 2.71 |
| G980 | 1.60 |
| G1010 | 0.90 |

The XRD pattern of Inconel 718 alloy shows the diffraction peaks of δ and γ phases. However, the strongest diffraction peak (112) of γ″ phase overlaps with the diffraction peak (111) of γ phase. Given that γ′ phase is an ordered phase of γ phase and the contents of γ″ and γ′ phases are low, the independent diffraction peaks of γ″ and γ′ phases cannot be ob-

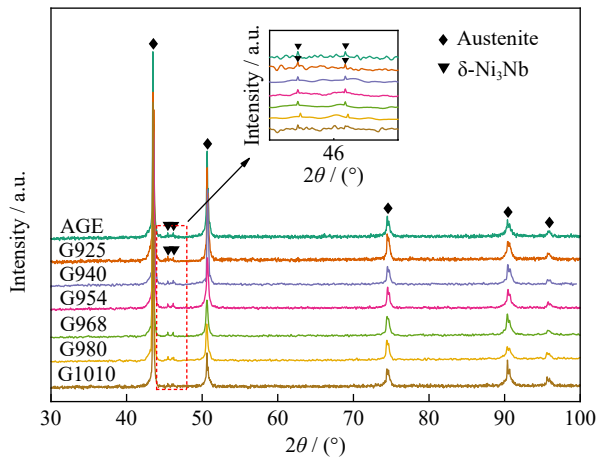


**Fig. 4. XRD diffraction patterns of Inconel 718 alloy under different heat treatment conditions.**

served. In addition, the diffraction peaks of NbC cannot be observed due to its small content. The following relationship can be obtained by XRD direct comparison [34]:

$$W_{\mathrm{NbC}} + W_{\delta} + W_{\gamma''} + W_{\gamma'} + W_{\gamma} = 1 \tag{1}$$

$$\frac{W_{\gamma'} + W_{\gamma}}{W_{\delta}} = \frac{\rho_{\gamma}}{\rho_{\delta}} \cdot \frac{\frac{1}{n}\sum_i^n \left(\frac{I_i^{\gamma}}{R_i^{\gamma}}\right)}{\frac{1}{m}\sum_i^m \left(\frac{I_i^{\delta}}{R_i^{\delta}}\right)} \tag{2}$$

$$\frac{W_{\mathrm{NbC}}}{W_{\delta}} = \frac{\rho_{\mathrm{NbC}}}{\rho_{\delta}} \cdot \frac{\frac{I_{111}^{\mathrm{NbC}}}{R_{111}^{\mathrm{NbC}}}}{\frac{1}{m}\sum_i^m \left(\frac{I_i^{\delta}}{R_i^{\delta}}\right)} \tag{3}$$

where $W_{\mathrm{NbC}}$, $W_{\delta}$, $W_{\gamma''}$, $W_{\gamma'}$, and $W_{\gamma}$ are the weight percentages of NbC, δ, γ″, γ′, and γ phases, respectively. $\rho_{\mathrm{NbC}}$, $\rho_{\delta}$, and $\rho_{\gamma}$ are the densities of NbC, δ, and γ phases, respectively. $I_{111}^{\mathrm{NbC}}$, $I_i^{\delta}$, and $I_i^{\gamma}$ are the integral intensities of the diffraction peaks of NbC, δ, and γ phases, respectively. $n$ and $m$ are the numbers of the diffraction peaks of δ and γ phases, respectively. The integral intensity of the diffraction peaks of γ phase in Eq. (2) includes that of the diffraction peaks of γ′ phase. $R_i$ is a value that calculates the integral intensity of the diffraction peak of a phase and is related to the specific phase. Assuming that the $R_i$ value of γ phase is equal to that of γ′ phase, $R_i$ can be expressed as follows:

$$R_i = \frac{1}{v^2} P_i F_i^2 \varphi(\theta) \mathrm{e}^{-2M} \tag{4}$$

where $v$ is the unit cell volume, and $F$ is the structure factor calculated according to Inconel 718 alloy composition, δ phase composition, and NbC. $P$ is the multiplicity factor, $\varphi(\theta)$ is the angular factor, $\mathrm{e}^{-2M}$ is the temperature factor.

The relationship between austenite lattice constant and precipitate content in Inconel 718 alloy is [35]:

$$a = a_0 - \frac{(1.9647\times10^{-6}W_{\delta}) + (2.4093\times10^{-6}W_{\gamma''}) + (0.8435\times10^{-6}W_{\gamma'})}{m(m - 0.01526W_{\delta} - 0.01508 - 0.01718W_{\gamma'})} \tag{5}$$

where $a$ is austenite lattice constant and $a_0$ = 0.3608 nm.

In addition, the relationship between the contents of γ″ and γ′ phases in Inconel 718 alloy is [36–37]:

$$\frac{W_{\gamma''}}{W_{\gamma'}} = 4 \tag{6}$$

The content of each precipitated phase in Inconel 718 alloy can be measured by the above relationships, and the results are shown in Table 5. Given that the δ phase has dissolved in the G1010 sample and the corresponding XRD diffraction peaks cannot be found, the weight percentage of the δ phase is not calculated.

The weight percentage of the δ phase first increases and then decreases with the increase in the second-step solid solution temperature, and this trend is consistent with the statistical results of semiquantitative analysis by Image Pro software. The content of γ″ phase decreases first and then increases, and those of γ′ and γ phases remain unchanged.

**Table 5. Weight percentage of each precipitate under different heat treatment conditions** wt%

| Sample | $W_{\delta}$ | $W_{\gamma''}$ | $W_{\gamma'}$ | $W_{\gamma}$ |
|---|---|---|---|---|
| AGE | 2.10 | 9.44 | 2.36 | 86.10 |
| G925 | 3.28 | 8.90 | 2.23 | 85.59 |
| G940 | 3.56 | 8.70 | 2.17 | 85.57 |
| G954 | 4.78 | 8.17 | 2.04 | 85.01 |
| G968 | 3.45 | 8.79 | 2.20 | 85.56 |
| G980 | 2.27 | 9.38 | 2.35 | 86.01 |

These results show that the different second-step solid solution temperature mainly affects the precipitation of γ″ and δ phases, and the contents of γ″ and δ phases have opposite trends.

The TEM images of Inconel 718 alloy with different heat treatment states are shown in Fig. 5. Fig. 5(f) illustrates that the elliptical precipitates in γ matrix are γ′ and γ″ phases. Compared with those in the original forged state, the size and content of precipitated γ″ phase significantly increase after the two-step solid solution treatment. Coarsened γ″ phase is observed in Fig. 5(c) and (d). The coarsening kinetics of γ″ precipitates theoretically follows the classical LSW model [38–39]. After γ″ phase nucleation inside the grain, the Ni and Nb around γ″ phase are still supersaturated, and γ″ phase continues to grow. However, due to the high content of δ phase precipitated at the grain boundaries in G925 and G954, some δ phases grow into the γ matrix by consuming Ni and Nb. As a consequence, the supersaturation of these two elements in the matrix is minimized. In this case, the growth of γ″ phase is inhibited. According to Ostwald ripening law, abundant interfaces between precipitates and parent phases lead to excessive interfacial energy. For interfacial energy reduction, the coarsening of γ″ phase occurs; that is, small-sized γ″ phase dissolves into the matrix, providing forming elements and conditions for the coarsening of large-sized γ″ phase. In the forged state, the δ phase content in the AGE and G1010 samples is low so the Ni and Nb contents in the matrix remain high. Instead of coarsening, the γ″ phases continue to nucleate and grow. Therefore, coarsening is not observed in the heat-treated samples in Fig. 5(a), (b), and (e).

### 3.2. Precipitation behavior of δ phase

3.2.1. Nucleation and growth of δ phase

The high-magnification bright-field (BF) TEM images of Inconel 718 alloy were obtained to study the evolution of δ phase morphologies near the grain boundaries of Inconel 718 alloy after different two-step solid solution treatments as shown in Fig. 6. Red and yellow arrows represent grain boundaries (GBs) and needle-like δ phases, respectively. For the AGE sample, many elliptical black spots appear in the matrix, and rod-shaped precipitated particles nucleate at the grain boundaries. As shown in the SAED image in Fig. 6(a), this precipitation at grain boundaries is the δ phase. The orientation relationship between the δ phase and γ matrix is $[01\bar{1}]_{\gamma}//[\bar{1}02]_{\delta}$. In general, the δ phase precipitates incoherently on the γ-matrix along {111} planes. Vacancies, disloca-

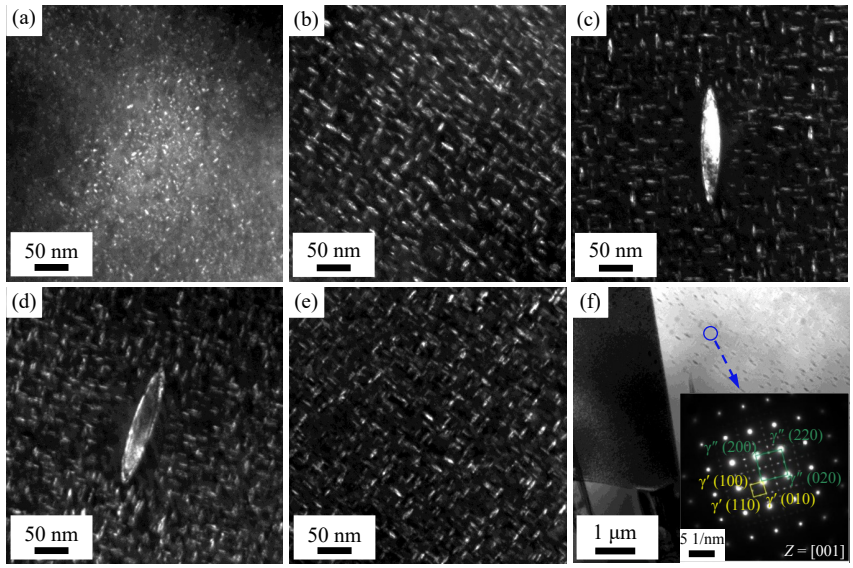


**Fig. 5. TEM images of Inconel 718 alloy with different heat treatment states: (a) as forged state, (b) AGE, (c) G925, (d) G954, and (e) G1010; (f) TEM image of G925 and selected area electron diffraction (SAED) image of γ″ and γ′ phases.**

tions, stacking faults (SFs), and grain boundaries in the γ matrix are commonly applied as the preferential nucleation sites of the δ phase [40]. Among them, grain boundaries can provide good thermodynamic and kinetic conditions and reduce the activation energy for the nucleation of the δ phase. Therefore, the δ phase always preferentially nucleates at grain boundaries and grows along grain boundaries under Nb diffusion. In Fig. 6(b), some needle-like δ phase appears in G925 and grows from the grain boundaries into γ grain. In addition, the growth direction of the needle-like δ phase forms a large angle with grain boundaries [28]. Needle-like δ phase often forms a large angle with the grain boundaries because it cannot find a suitable phase plane parallel to the grain boundaries.

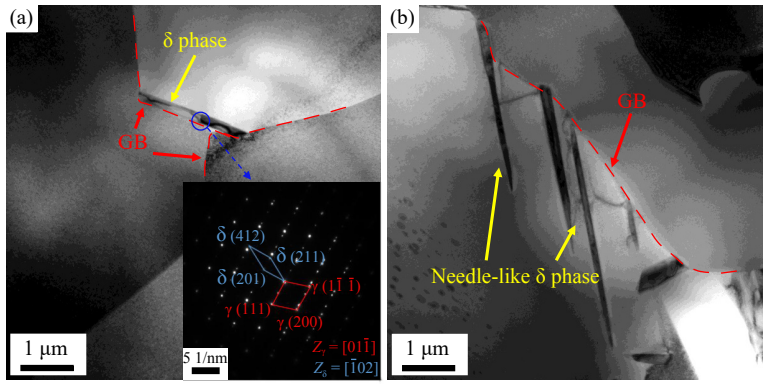


**Fig. 6. BF TEM images of Inconel 718 alloy: (a) TEM image of AGE and SAED image of γ and δ phases; (b) TEM image of G925.**

With the increase in the second-step solid solution temperature, the δ phase precipitates gradually and its content increases. Aggregation occurs during its growth. The plate-like δ phases grown along the same orientation are connected to each other to form a special "linear arrangement" form [41]. In the two-step solid solution treatment, a small amount of elongated needle-like δ phase is found in the grain, as shown in Fig. 7(a). As illustrated in the SAED image in Fig. 7(b), the orientation relationship between the intragranular δ phase and γ matrix is $[\bar{1}00]_\delta // [01\bar{1}]_\gamma$ and $(010)_\delta // (111)_\gamma$. This finding shows that the γ″ phase is absent in the intracrystalline part around the δ phase grown in the grain or grain boundaries. This phenomenon can be explained in two ways. First, given that the forming elements of δ phase and γ″ phase are the same and the precipitated δ phase consumes a large amount of Ni and Nb, the γ″ phase cannot be formed near the δ phase. Second, when the δ phase saturates the grain boundaries and a large amount of Ni and Nb have been occupied by the γ″ phase, the γ″ phase is changed by SFs and transforms into the δ phase to continuously precipitate δ phase in the grain.

3.2.2. Transformation from γ″ to δ phase

Coarsened γ″ phase and intracrystalline δ phase were found in the G925 and G954 samples but not found in the other heat-treated samples. Given that the aging time and temperature of each group are consistent, this coarsening behavior of γ″ phase could promote the precipitation of δ phase inside the grain. The structure of the γ″ phase changes due to the SFs after coarsening, and the γ″ phase transforms to the δ phase, resulting in the formation of δ phase at the interior of austenite grain.

Fig. 8 shows the high-resolution transmission electron microscopy (HRTEM) and inverse fast Fourier transform

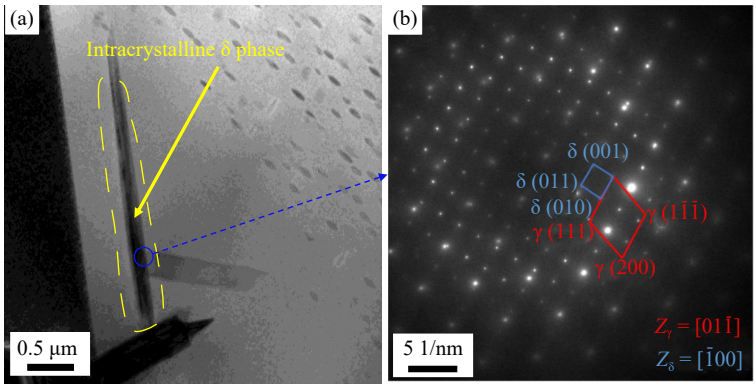


**Fig. 7. (a) TEM images of intracrystalline δ phase in G925, and (b) the corresponding SAED image of γ and δ phases.**

(IFFT) images of γ″ phase in G925. Atomic mismatches and SFs are found around the γ″ phase particles. The existence of these defects provides the possibility for the transformation of the γ″ phase to the δ phase.

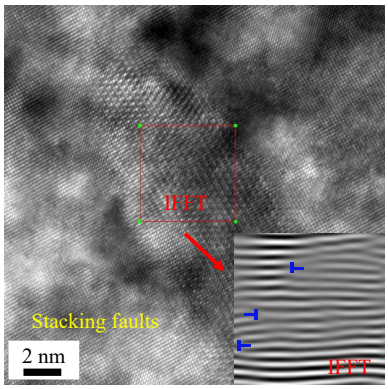


**Fig. 8. HRTEM and IFFT images of γ″ phase in G925.**

γ″ phase is a body-centered tetragonal $D0_{22}$ structure [28], and its unit cell can be seen as two stacked cells of $L1_2$ structure along a cubic axis, featuring an inverted domain boundary in the middle. Nb atoms occupy eight corners and body center positions, and Ni atoms occupy face center and edge center positions parallel to the *c*-axis. The unit cell structure is shown in Fig. 9(a). In the $D0_{22}$ structure, the close-packed surface is (112), and each six-layer close-packed surface completes a stacking cycle. The distance of each layer is equivalent to a 1/3 (121) slip distance. The atomic layer stacking order is $A_1B_1C_1A_2B_2C_2A_1B_1C_1$…

A large distortion occurs when the γ″ phase precipitates from the γ matrix, resulting in dislocation on the close-packed surface (112) of the γ″ phase. These close-packed surfaces in the γ″ phase further result in SFs, and the stacking sequence is $A_1B_1C_1A_2B_2C_2A_1B_1C_1$… When a δC-type dislocation slips across the $B_1$ plane, the atoms of $B_1$ plane move the displacement of $a/6$ [11$\bar{2}$], where *a* is austenite lattice constant, resulting in a new stacking order of $A_1B_1C_1A_2B_2C_2A_1C_2A_1B_1C_1A_2B_2C_2$… The SFs are formed by these four continuous CACA stacking $A_3$-type structures, which are the structural characteristics of the δ phase, that is, the transformation of the γ″ phase to the δ phase [28,38]. Fig. 9(b) explains the nucleation mode of δ phase at SFs in γ″ phase.

### 3.3. Hardness test

The Vickers hardness of Inconel 718 alloy with different two-step solid solution treatment states is shown in Fig. 10. Compared with that at the as-forged state, the hardness is significantly increased after the solid solution treatment. With the increase in the second-step solid solution temperature, the hardness first decreases and then increases. The hardness of the sample treated by the second-step solid solution at 1010°C reaches a maximum value of HV 446.84. In this case, the δ phase mostly dissolves into the matrix after solution treatment at 1010°C. The large amount of δ phase dissolution leads to an increase in Ni and Nb in the matrix, which in turn increases the amount of γ″ phase precipitation. Although the grain size is the largest at 1010°C, the great strengthening effect of the γ″ phase makes up for the decrease in hardness caused by grain growth. Therefore, the

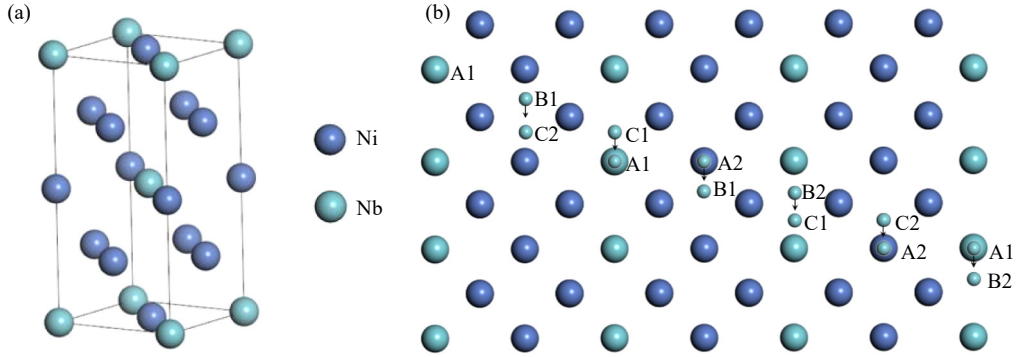


**Fig. 9. Schematic of δ phase formation mode: (a) unit cell of γ″ phase with $D0_{22}$ structure; (b) arrangement of Nb atoms in consecutive close-packed planes of γ″ phase after the passage of an $a/6$ [11$\bar{2}$] partial dislocation.**

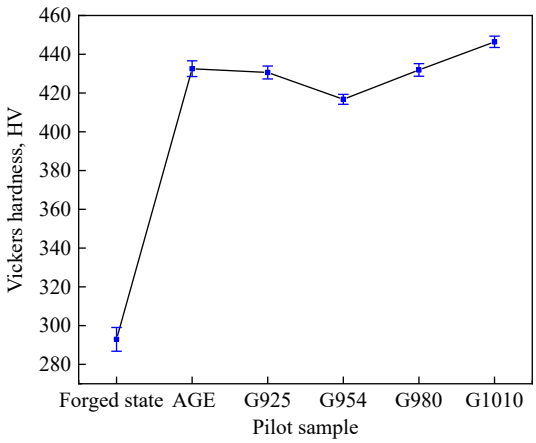


**Fig. 10. Vickers hardness of Inconel 718 alloy with different two-step solid solution treatments.**

hardness is the largest at 1010°C.

Owing to the significant strengthening effect and high content of the γ″ phase, the overall hardness does not change much under the different two-step solid solution treatments. Given that the δ phase is not a strengthening phase, an increase in its content consumes Nb, leading to a decrease in the precipitation of the γ″ phase. This phenomenon manifests as a decrease in hardness. The hardness of G980 and AGE does not change much mainly because the contents of δ and γ″ phases in the two specimens are almost same and the hardness of G980 is HV 432.35. According to the results in Table 4, in the range of 925–960°C, the higher the second-step solid solution temperature, the more conducive to δ phase precipitation, resulting in the decrease of γ″ phase precipitation. The two-step solid solution treatment in this temperature range also causes γ″ phase coarsening, resulting in a reduction in precipitation strengthening manifested as a decrease in hardness. At a high second-step solid solution temperature over 980°C, the δ phase dissolves back into the matrix, and the γ″ phase precipitates increase after aging. Therefore, the precipitation strengthening effect is enhanced as manifested by an increase in hardness. In addition, the increase in hardness after the second-step solid solution treatment between 980 and 1010°C is significantly higher than that between 925 and 960°C, indicating that the significant dissolution temperature of the δ phase of Inconel 718 alloy is in the range of 980–1010°C under this composition.

## 4. Conclusions

The effects of a new two-step solid solution treatment on the microstructure and precipitates of Inconel 718 alloy were studied. The evolution of δ phase during the two-step solid solution treatment was examined, and the transformation mechanism from γ″ metastable phase to δ phase was clarified. This study provides the following key findings that contribute to a comprehensive understanding of Inconel 718 alloy precipitation during the two-step solid solution treatment.

(1) With the increase in the second-step solid solution temperature, the average grain diameter of Inconel 718 alloy decreases first, then increases and finally stabilizes. This trend is due to the pinning effect of the δ phase precipitated on the grain boundaries.

(2) The number of δ phases with short rod shape at the grain boundaries and needle shape in the grain interior increase first and then decrease with the increase in the second-step solid solution temperature. The hardness of the material treated at 1010°C reaches a maximum value of HV 446.84.

(3) Intragranular δ phase appears in the sample subjected to the second-step solid solution treatment at 925°C, and the orientation relationship with γ matrix is $[\bar{1}00]_\delta//[01\bar{1}]_\gamma$ and $(010)_\delta//(111)_\gamma$. The formation of this intragranular δ phase, that is, the transformation from γ″ metastable phase to δ phase, was explained by SF theory.

## Acknowledgements

This work was financially supported by the National Natural Science Foundation of China (Nos. 52201203 and 52171107), the Hebei Provincial Natural Science Foundation, China (No. E2021501026), the National Natural Science Foundation of China-Joint Fund of Iron and Steel Research (No. U1960204), and the “333” Talent Project of Hebei Province, China (No. B20221001).

## Conflict of Interest

The authors declare that they have no known competing financial interests or personal relationships that could have appeared to influence the work reported in this paper.

## References

[1] F. Theska, A. Stanojevic, B. Oberwinkler, and S. Primig, Microstructure-property relationships in directly aged Alloy 718 turbine disks, *Mater. Sci. Eng. A*, 776(2020), art. No. 138967.

[2] A. Balan, M. Perez, T. Chaise, *et al*., Precipitation of γ″ in Inconel 718 alloy from microstructure to mechanical properties, *Materialia*, 20(2021), art. No. 101187.

[3] H. He, L. Yu, C. Liu, H. Li, Q. Gao, and Y. Liu, Research progress of a novel martensitic heat-resistant steel G115, *Acta Metall. Sin.*, 58(2022), No. 3, p. 311.

[4] A. De Bartolomeis, S.T. Newman, I.S. Jawahir, D. Biermann, and A. Shokrani, Future research directions in the machining of Inconel 718, *J. Mater. Process. Technol.*, 297(2021), art. No. 117260.

[5] E.M. Fayed, D. Shahriari, M. Saadati, V. Brailovski, M. Jahazi, and M. Medraj, Influence of homogenization and solution treatments time on the microstructure and hardness of inconel 718 fabricated by laser powder bed fusion process, *Materials*, 13(2020), No. 11, art. No. 2574.

[6] H.J. Zhang, C. Li, Q.Y. Guo, *et al*., Hot tensile behavior of cold-rolled Inconel 718 alloy at 650 °C: The role of δ phase, *Mater. Sci. Eng. A*, 722(2018), p. 136.

[7] Q.Z. Gao, Z.Y. Liu, L.L. Sun, *et al*., Review on precipitates and high-temperature properties of alumina-forming austenitic stainless steel, *J. Mater. Res. Technol.*, 25(2023), p. 5372.

[8] J. Ding, S. Xue, Z. Shang, *et al*., Characterization of precipitation in gradient Inconel 718 superalloy, *Mater. Sci. Eng. A*, 804(2021), art. No. 140718.

[9] G.H. Cao, T.Y. Sun, C.H. Wang, *et al*., Investigations of γ′, γ″ and δ precipitates in heat-treated Inconel 718 alloy fabricated by

selective laser melting, *Mater. Charact.*, 136(2018), p. 398.
[10] D. Sindhura, M.V. Sravya, and G.V.S. Murthy, Comprehensive microstructural evaluation of precipitation in Inconel 718, *Metallogr. Microstruct. Anal.*, 8(2019), No. 2, p. 233.
[11] D. Srinivasan, Effect of long-time exposure on the evolution of minor phases in Alloy 718, *Mater. Sci. Eng. A*, 364(2004), No. 1-2, p. 27.
[12] S.A. Mantri, S. Dasari, A. Sharma, *et al*., Effect of micro-segregation of alloying elements on the precipitation behaviour in laser surface engineered Alloy 718, *Acta Mater.*, 210(2021), art. No. 116844.
[13] Y.P. Mei, Y.C. Liu, C.X. Liu, *et al*., Effects of cold rolling on the precipitation kinetics and the morphology evolution of intermediate phases in Inconel 718 alloy, *J. Alloys Compd.*, 649(2015), p. 949.
[14] S. Azadian, L.Y. Wei, and R. Warren, Delta phase precipitation in Inconel 718, *Mater. Charact.*, 53(2004), No. 1, p. 7.
[15] D.H. Ping, Y.F. Gu, C.Y. Cui, and H. Harada, Grain boundary segregation in a Ni–Fe-based (Alloy 718) superalloy, *Mater. Sci. Eng. A*, 456(2007), No. 1-2, p. 99.
[16] M. Anderson, A.L. Thielin, F. Bridier, P. Bocher, and J. Savoie, δ Phase precipitation in Inconel 718 and associated mechanical properties, *Mater. Sci. Eng. A*, 679(2017), p. 48.
[17] R.S. Huang, Y.A. Sun, L.L. Xing, G.L. Song, W. Liu, and Q.L. Li, Effect of gradient microstructure pinned by δ phase on elevated temperature performances of GH4169, *Mater. Sci. Eng. A*, 774(2020), art. No. 138913.
[18] E.M. Fayed, M. Saadati, D. Shahriari, V. Brailovski, M. Jahazi, and M. Medraj, Effect of homogenization and solution treatments time on the elevated-temperature mechanical behavior of Inconel 718 fabricated by laser powder bed fusion, *Sci. Rep.*, 11(2021), art. No. 2020.
[19] K.S. Prasad, S.K. Panda, S.K. Kar, S.V.S.N. Murty, and S.C. Sharma, Prediction of fracture and deep drawing behavior of solution treated Inconel-718 sheets: Numerical modeling and experimental validation, *Mater. Sci. Eng. A*, 733(2018), p. 393.
[20] W.D. Song, M.L. Hu, H.S. Zhang, and Y.X. Jin, Effects of different heat treatments on the dynamic shear response and shear localization in Inconel 718 alloy, *Mater. Sci. Eng. A*, 725(2018), p. 76.
[21] N.Y. Ye, M. Cheng, S.H. Zhang, H.W. Song, and H.W. Zhou, Influence of delta phase precipitation on static recrystallization of cold-rolled Inconel 718 alloy in solid solution treatment, *J. Iron Steel Res. Int.*, 26(2019), No. 2, p. 148.
[22] X.G. You, Y. Tan, S. Shi, *et al*., Effect of solution heat treatment on the precipitation behavior and strengthening mechanisms of electron beam smelted Inconel 718 superalloy, *Mater. Sci. Eng. A*, 689(2017), p. 257.
[23] X.G. You, Y. Tan, L.H. Zhao, *et al*., Effect of solution heat treatment on microstructure and electrochemical behavior of electron beam smelted Inconel 718 superalloy, *J. Alloys Compd.*, 741(2018), p. 792.
[24] P.K. Bai, P.C. Huo, J. Wang, *et al*., Microstructural evolution and mechanical properties of Inconel 718 alloy manufactured by selective laser melting after solution and double aging treatments, *J. Alloys Compd.*, 911(2022), art. No. 164988.
[25] G.A. Rao, M. Srinivas, and D.S. Sarma, Effect of solution treatment temperature on microstructure and mechanical properties of hot isostatically pressed superalloy Inconel* 718, *Mater. Sci. Technol.*, 20(2004), No. 9, p. 1161.
[26] X.L. An, L. Zhou, B. Zhang, *et al*., Inconel 718 treated with two-stage solution and aging processes: Microstructure evolution and enhanced properties, *Mater. Res. Express*, 6(2019), No. 7, art. No. 075803.
[27] F. Theska, K. Nomoto, F. Godor, *et al*., On the early stages of precipitation during direct ageing of alloy 718, *Acta Mater.*, 188(2020), p. 492.
[28] M. Sundararaman, P. Mukhopadhyay, and S. Banerjee, Precipitation of the δ-$Ni_3Nb$ phase in two nickel base superalloys, *Metall. Trans. A*, 19(1988), No. 3, p. 453.
[29] C.H. Xiang, P.Z. Wang, X. Yang, and S.H. An, Effect of secondary solid solution treatment on microstructure and properties of IN718 alloy, *Heat Treat. Met.*, 46(2021), No. 6, p. 132.
[30] W. Le, Z.W. Chen, K. Yan, *et al*., Early evolution of δ phase and coarse γ″ phase in Inconel 718 alloy with high temperature ageing, *Mater. Charact.*, 180(2021), art. No. 111403.
[31] S.H. Chang, *In situ* TEM observation of γ′, γ″ and δ precipitations on Inconel 718 superalloy through HIP treatment, *J. Alloys Compd.*, 486(2009), No. 1-2, p. 716.
[32] M. Dehmas, J. Lacaze, A. Niang, and B. Viguier, TEM study of high-temperature precipitation of delta phase in Inconel 718 alloy, *Adv. Mater. Sci. Eng.*, 2011(2011), No. 1, art. No. 940634.
[33] Y.R. Sun, J. Wang, J. Yang, S.L. Wang, L. Liu, and L. Wei, Effect of heat treatment on microstructure and mechanical properties of IN718 deformed alloy, *Heat Treat. Met.*, 43(2018), No. 12, p. 152.
[34] W.C. Liu, F.R. Xiao, M. Yao, Z.L. Chen, S.G. Wang, and W.H. Li, Quantitative phase analysis of Inconel 718 by X-ray diffraction, *J. Mater. Sci. Lett.*, 16(1997), No. 9, p. 769.
[35] W.C. Liu, F.R. Xiao, M. Yao, Z.L. Chen, Z.Q. Jiang, and S.G. Wang, Relationship between the lattice constant of ϒ phase and the content of δ phase, γ″ and γ′ phases in inconel 718, *Scripta Mater.*, 37(1997), No. 1, p. 59.
[36] D.Y. Cai, W.C. Liu, R.B. Li, W.H. Zhang, and M. Yao, On the accuracy of the X-ray diffraction quantitative phases analysis method in Inconel 718, *J. Mater. Sci.*, 39(2004), No. 2, p. 719.
[37] W.C. Liu, M. Yao, Z.L. Chen, Z.Q. Jiang, S.G. Wang, and W.H. Li, Quantitative phase analysis of Inconel 718 alloy, *J. Aeronaut. Mater.*, 17(1997), No. 1, p. 17.
[38] K. Kusabiraki, S. Saji, and T. Tsutsumi, Effects of cold rolling and annealing on the structure of γ″ precipitates in a Ni–18Cr–16Fe–5Nb–3Mo alloy, *Metall. Mater. Trans. A*, 30(1999), No. 8, p. 1923.
[39] H.L. Qin, Z.N. Bi, H.Y. Yu, G. Feng, J.H. Du, and J. Zhang, Influence of stress on γ″ precipitation behavior in Inconel 718 during aging, *J. Alloys Compd.*, 740(2018), p. 997.
[40] H.J. Zhang, C. Li, Y.C. Liu, *et al*., Effect of hot deformation on γ″ and δ phase precipitation of Inconel 718 alloy during deformation&isothermal treatment, *J. Alloys Compd.*, 716(2017), p. 65.
[41] H.J. Zhang, C. Li, Q.Y. Guo, *et al*., Delta precipitation in wrought Inconel 718 alloy; the role of dynamic recrystallization, *Mater. Charact.*, 133(2017), p. 138.